NUMERICAL SIMULATIONS OF FULLY NONLINEAR WAVE MOTIONS IN A DIGITAL WAVE TANK

J.C. Park[1] and K.S. Kim[*2]

디지털 파랑 수조 내에서의 비선형 파랑 운동의 수치시뮬레이션

박 종 천[1], 김 경 성[*2]

A digital wave tank (DWT) simulation technique has been developed by authors to investigate the interactions of fully nonlinear waves with 3D marine structures. A finite-difference/volume method and a modified marker-and-cell (MAC) algorithm have been used, which are based on the Navier-Stokes (NS) and continuity equations. The fully nonlinear kinematic free-surface condition is implemented by the marker-density function (MDF) technique or the Level-Set (LS) technique developed for one or two fluid layers. In this paper, some applications for various engineering problems with free-surface are introduced and discussed. It includes numerical simulation of marine environments by simulation equipments, fully nonlinear wave motions around offshore structures, nonlinear ship waves, ship motions in waves and marine flow simulation with free-surface. From the presented simulations, it seems that the developed DWT simulation technique can handle various engineering problems with free-surface and reliably predict hydrodynamic features due to the fully-nonlinear wave motions interacting with such marine structures.

Key Words : Digital wave tank (DWT), Nonlinear wave motions, Navier-Stokes (N-S) equation, Ship motion simulation, Numerical wavemaker, Wave-structure interaction

1. INTRODUCTION

Virtual reality by use of computational fluid dynamics (CFD) has been realized by high accuracy of simulation technique and high performance of computer power. Especially, System-Design-By-Simulation techniques for marine structures are quite effective for design of the structures, based on understanding of physical phenomena. Of these, a digital wave tank (DWT) simulation techniques have been also developed to more advanced technology, and it can be first utilized for the purpose of elucidating nonlinear physical phenomena related to nonlinear wave motions, and then applied to the purpose of designing or inventing new systems in ocean or coasts. In near future, as shown in Fig. 1, it is believed that all experimental towing tank tests would be alternated with digital towing tank tests, including not only resistance tests but also motion and maneuvering tests in random sea conditions.

However, the numerical implementation of the fully nonlinear free-surface condition is in general complicated and difficult. The major difficulties associated with the fully nonlinear free-surface simulations around 3D structures consist in (i) the complicated nonlinear free-surface boundary conditions that have to be satisfied on the instantaneous free-surface position not known a priori, (ii) various types of numerical instabilities, (iii) the appropriate open-boundary conditions representing open-sea condition, (iv) the treatment of body-surface condition of complex geometry in the vicinity of free-surface, and (v) large CPU time and storage required to keep satisfactory degree of accuracy.

In the present study, efforts have been focused on the nonlinear free-surface motions using a marker-density function

접수일: 2006년 11월 6일, 심사완료일: 2006년 11월 13일.
1 정회원, 부산대학교 조선해양공학과
2 학생회원, 부산대학교 조선해양공학과
* Corresponding author, E-mail: jcpark@pusan.ac.kr

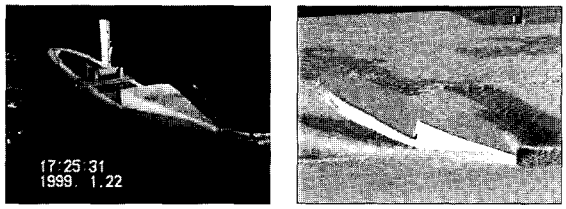

Fig. 1 Ship model tests in an experomental tank (left) and a DWT (right).

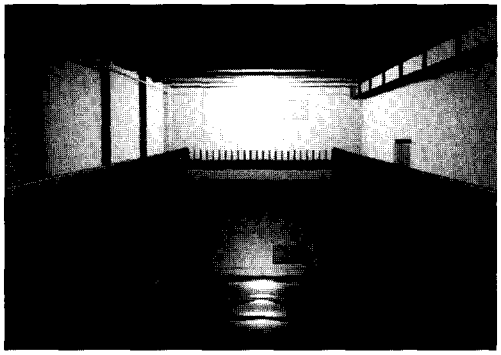

Fig. 2 Schematic view of DWT

(MDF) method. The method is basically similar to the volume-of-fluid (VOF) method (Hirt and Nichols, 1981) in that the interface can be defined by the volume fraction of fluid within a cell. However, the numerical treatment of the MDF method is more easily applicable to complicated free-surface flows around a 3D body. The MDF technique was originally devised by Miyata et al. (1988) to cope with two-layer flows involving strongly interacting interface. However, the accuracy of the method in the wave formation was not fully verified at that time. Park et al. (1993) improved the accuracy of the interface treatment through numerical experiments with non-breaking regular periodic waves. The technique has since been upgraded and used for various engineering problems including the 2D breaking waves (Park & Miyata, 1994), 3D breaking waves around a ship and an offshore structure (Miyata & Park, 1995; Miyata et al., 1996; Sato et al, 1999; Orihara & Miyata, 2000), the fully-nonlinear DWT simulations (Park et al., 1999 & 2003; Kim et al., 2000), the bubbly flow (Kanai & Miyata, 2001), etc. Similar methods using the same MDF concept have been developed recently, which include the continuum surface force (CSF) method by Brackbill et al. (1992), the CIP method by Yabe et al. (1993), and the level-set method by Sussman et al. (1994).

In the present study, emphasis is put on a DWT simulation technique and their applications. The numerical simulation method for the DWT is briefly introduced in Sec.2. The capability of the simulation equipments of marine environments are demonstrated in Sec.3. In Sec.4, various applications for the engineering problems with fully-nonlinear wave motions are introduced. Some concluding remarks are given in Sec.5.

2. NUMERICAL IMPLEMENTATION OF DWT

2.1 DWT SIMULATION TECHNIQUES

Fig. 2 shows a schematic view of a DWT, and the outline of the developed DWT simulation technique is summarized in Table.1. The governing equations, Navier-Stokes (N-S) and continuity equations, are solved in the computational domain and the boundary values updated at each time step by a finite-difference/ volume time-marching scheme in the framework of rectangular/curvilinear coordinate system. The nonlinear free-surface configuration is mainly determined by the MDF technique. For the turbulence model, SGS model is employed. And for the convective terms a flux-split method similar to a third-order TVD scheme with limiter is used. The second-order Adams-Bashforth method is used for the time-differencing. A second-order central differencing scheme is employed for the diffusive terms.

The solution algorithm can be referred from Park et al.(1999 & 2003), Miyata & Park(1995), Sato et al.(1999).

2.2 NONLINEAR FREE SURFACE CONDITIONS

The most important conditions for the free surface are the kinematic and dynamic conditions.

In case the variables of density ρ , velocity v, normal vector n and infinitesimally small free-surface segment ds are defined as

Table 1 Outline of the developed DWT Simulation Technique.

• Finite-Difference/Volume Method.
• Modified-MAC algorithm.
• **H-H** *or* **O-H Grid System.**
• **SOR** iteration method for solving pressure field.
• **MDF** *or* **LS** technique for nonlinear free-surface movement.
• **Large-Eddy-Simulation** *or* **RANS** for turbulent flow *with wall function.*
• 3rd-order **TVD scheme** *with limiter* for Advection Term.
• 2nd-order **Adams-Bashforth** scheme for time integration.

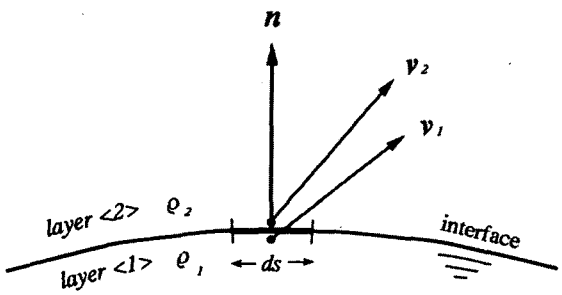

Fig .3 Definition of velocity and normal component vectors on the interface

shown in Fig. 3, the conservation of mass across ds becomes

$$\rho_1 v_1 \cdot n = \rho_2 v_2 \cdot n \tag{1}$$

Suppose that two fluids are not mixed and then

$$v_1 \cdot n = v_2 \cdot n \tag{2}$$

that is

$$(v_1 - v_2) \cdot n = 0 \tag{3}$$

Eq. (3) is the kinematic condition on the free-surface boundary, which means that fluid particles on the free surface remain on the same boundary.

When the free surface is assumed to be a function of horizontal coordinate (x,y) and time t as

$$F(x,y,t) = h_0; const \tag{4}$$

and the kinematic condition in the Eulerian coordinate system becomes

$$\frac{DF}{Dt}(x,y,t) = 0 \tag{5}$$

where substantial (total) differentiation is used.

The kinematic condition by use of Lagrangian coordinate system is

$$\frac{D\xi}{Dt} = u, \quad \frac{D\eta}{Dt} = v \tag{6}$$

where (ξ,η) is the Lagrangian coordinate on the free-surface and (u,v) is the components of velocity.

To implement the kinematic free-surface condition and to determine the free-surface configuration, the MDF M_ρ is used in the present study. Two-layer flows are considered and the density of the fluid in the lower and upper layers is denoted by ρ_1 and ρ_2.The MDF is governed by the following transportation equation.

$$\frac{\partial M_\rho}{\partial t} + u\frac{\partial M_\rho}{\partial x} + v\frac{\partial M_\rho}{\partial y} + w\frac{\partial M_\rho}{\partial z} = 0 \tag{7}$$

where the MDF M_ρ takes the value between 0 and 1 all over the computational domain. The scalar value has the meaning of porosity in each cell. Eq. (7) is calculated at each time step and the free-surface location is determined by the position where the MDF takes the mean value as

$$\overline{M_\rho} = 0.5 \tag{8}$$

The interface location $\overline{M_\rho}$ is the same as the wave height function h in general unless overturning breaking waves are considered. Thus, Eq. (7) is more general and solved for the movement of fluid interface.

From the law of momentum conservation, the following dynamic conditions are derived in the normal n and tangential τ directions, respectively (Levich & Krylov, 1969).

$$p_1 - p_2 + \gamma\kappa = 2\mu_1\frac{\partial v_1^n}{\partial n} - 2\mu_2\frac{\partial v_2^n}{\partial n} \tag{9}$$

$$\mu_1\left(\frac{\partial v_1^n}{\partial \tau} + \frac{\partial v_1^\tau}{\partial n}\right) - \mu_2\left(\frac{\partial v_1^n}{\partial \tau} + \frac{\partial v_1^\tau}{\partial n}\right) = \frac{\partial \gamma}{\partial \tau} \tag{10}$$

Here, γ is the surface tension, κ the radius of curvature, μ the dynamic viscosity and p the pressure. The subscripts 1 and 2 denote the fluid 1 (lower layer) and fluid 2 (upper layer).

By assuming that viscous stress and surface tension on the free surface are negligible, the dynamic conditions can be written in the following simpler forms.

$$p_1 = p_2 \tag{11}$$

$$\mu_1\left(\frac{\partial v_1^\tau}{\partial n}\right) = \mu_2\left(\frac{\partial v_2^\tau}{\partial n}\right) \tag{12}$$

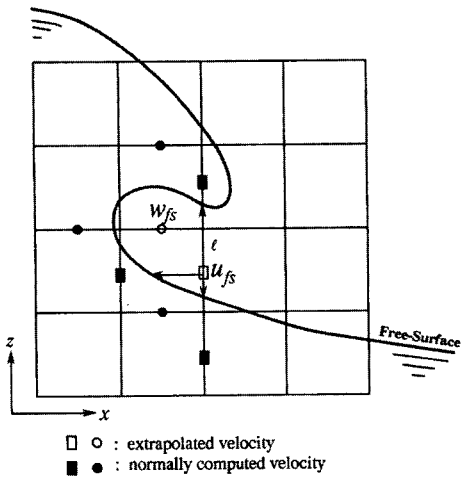

Fig. 4 Schematic sketch of velocity extrapolation for overturning motion at interface

The dynamic free-surface condition of Eq. (11) is implemented by the so-called "irregular star" technique (Chan & Street, 1970) in the solution process of the Poisson equation for the pressure. The pressure at the free-surface is determined by extrapolating with zero gradient in a direction approximately normal to the free surface and taking into consideration the static pressure difference in the vertical direction due to gravity. Similarly, velocities are extrapolated at the interface with approximately no normal gradient as

$$u_{fs} = \frac{\sum_k \left(\frac{u_k}{l_k}\right)}{\sum_k \left(\frac{1}{l_k}\right)} \tag{13}$$

where the subscript k is the number of velocities used in the extrapolation, u_k denotes the velocities in the lower layer and l the length between the position of the velocity u_k and the free-surface as shown in Fig. 4. This treatment is in gross accord with the viscous tangential condition of Eq. (12) at the free surface, and can cope with 3D overturning free-surface configuration.

2.3 OTHER BOUNDARY CONDITIONS

At the inflow boundary, i.e., the simulation equipments of marine environments, i.e. a numerical wavemaker, is established by prescribing the inflow velocities based on the water particle velocities of the linear wave (or Stokes second-order wave), which is like a flexible flap wavemaker. For multi-directional wave generation, a snake-like wavemaker motion is used on the basis of linear wavemaker theory (Dean and Darlymple, 1991). Fig. 5 indicates a procedure of imposing boundary condition on wave panels.

For the sidewall boundary, the diverse boundary conditions can be imposed flexibly. For instances, the free-slip rigid wall and the weakly-opened boundary conditions were tested in Kim et al. (2001), and one side of a dual-face-snake-type wavemaker with the other side of a numerical beach was employed to increase the effective test area in Kim et al. (2000).

One of the most critical issues for fully-nonlinear digital wave tank simulations is the numerical implementation of a robust downstream open boundary condition. A well-designed open boundary condition is particularly important to reduce the size of the computational domain. In the present study, an artificial damping scheme (Park et al., 1999) is employed in the added dissipation zone to dissipate all the wave energy of outgoing waves, and the mesh size is gradually increased in the horizontal direction to provide additional numerical damping.

At the bottom boundary of the DWT, zero-normal- gradient boundary conditions are given for the velocity and the hydrostatic pressure is given assuming that the vertical distances from the interface are sufficiently large in comparison with the wave height of interest.

No-slip body boundary condition is imposed on the body surface. A special treatment of the free-surface location at the intersection with the body surface has been made so that the possible singularity is removed, i.e. the values of MDF on the body surface are extrapolated with zero-normal gradient from the fluid region.

3. SIMULATION EQUIPMENTS OF MARINE ENVIRONMENTS

3.1 NUMERICAL SIMULATION OF IRREGULAR WAVE

Numerical simulation of irregular wave was made by superposing 64 wave components selected from the Bretschneider-Mitsuyasu-type wave energy spectrum modified by Goda (1987) for coastal zone, which is expressed as:

$$S(f) = 0.205 H_{1/3}^2 T_{1/3}^{-4} f^5 \exp\left[-0.75\left(T_{1/3} f\right)\right]^{-4} \tag{14}$$

where, f is the frequency, $H_{1/3}$ significant wave height, and

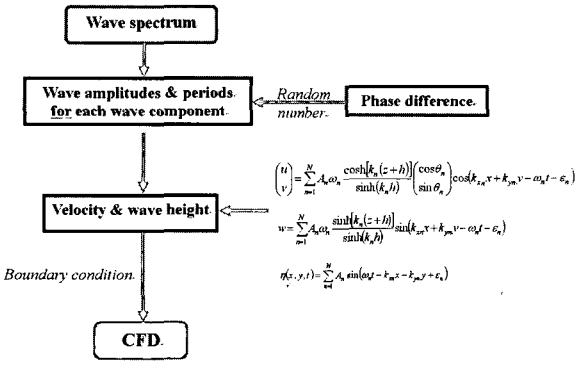

Fig. 5 Procedure of imposing boundary condition on wave panel

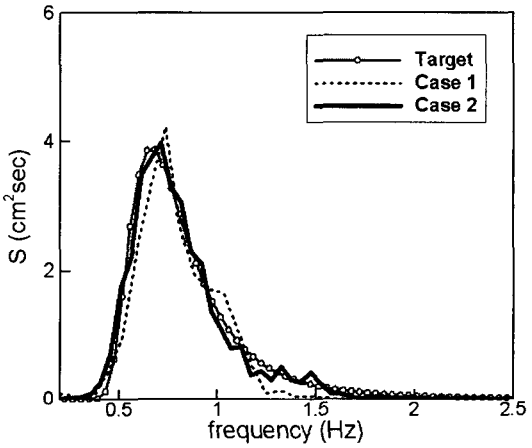

Fig. 6 Comparison of target and simulated wave spectra for 2D irregular wave

$T_{1/3}$ significant wave period. The wave amplitude of each component is calculated by $A=\sqrt{2S(f)df}$, wheredf is an interval of frequency between neighboring components. In this study, the significant wave height and period are set at $H_{1/3}$ =0.05m and $T_{1/3}$=1.33s, respectively.

Two cases of numerical simulation are tested with coarser (CASE 1) and finer (CASE 2) grid conditions, and the condition is detailed in Table 2.

In Fig. 6, the simulated wave spectra are quantitatively compared with the target spectrum. The spectral analysis is performed by FFT algorithm, which averaged through 5 times

Table 2 Condition of calculation for 2D irregular wave.

	CASE 1	CASE 2
Δx	$L_{1/3}$/50	$L_{1/3}$/150
Δz	$H_{1/3}$/20	$H_{1/3}$/20
Δt	$T_{1/3}$/800	$T_{1/3}$/2000

analyses with different phase angles. For CASE 2, overall agreement is excellent except for high frequency region ($f \gg 1.5Hz$) where the numerical dissipation of energy is remarkable.

3.2 NUMERICAL REPRODUCTION OF MULTI-DIRECTIONAL WAVE

In general a directional spectrum is represented by:

$$S(f;\theta)=S(f)\cdot G(\theta,f) \tag{15}$$

Here, $S(f)$ indicates frequency spectrum and $G(\theta,f)$ directional spreading function. In the present study, Eq. (16) is used for frequency spectrum and the Mitsuyasu-type function expressed in Eq. (18) is used for directional spreading function.

$$G(\theta,f)=G_0\cos^{2s}\left[(\theta-\theta_p)/2\right] \tag{16}$$

$$G_0=\left[\int_{\theta_{\min}}^{\theta_{\max}}\cos^{2s}(\theta/2)d\theta\right]^{-1} \tag{17}$$

$$s=\begin{cases}S_{\max}(f/f_p)^5 & : f\le f_p\\ S_{\max}(f/f_p)^{-2.5} & : f>f_p\end{cases} \tag{18}$$

where, θ is the azimuth measured counterclockwise from the principle wave direction, θ_p.And f_p the peak frequency (f_p= $T_{1/3}$/1.13), G_0 a constant to normalize the directional function, and s the directional wave energy spreading determined by angular spreading parameter $S_{\max}$(Goda&Suzuki, 1975).

As the computational condition, the 16×16 wave components are used for the components of frequency and wave angle. The length, width, and depth of the main DWT were 30m, 20m, and 2.8m, respectively. The longitudinal and lateral cell sizes were $\Delta x=\Delta y=L_{1/3}/20$, the vertical size $\Delta z=H_{1/3}/20$ and the sampling time $\Delta t=T_{1/3}/2000$.

A 3D snapshot of a numerically reproduced wave configuration at t=50s is shown in Fig. 7. The real sea random waves consisting of highly short-crest waves seem to be simulated and reproduced numerically well. However, the waves in far field from wavemaker are generated inadequately compare to those in near field from wavemaker, which are due to numerical dissipation.

Fig. 8 shows the numerically obtained contour map of directional spectrum analyzed by the extended maximum entropy principle (EMEP) method by Hashimoto et al. (1994). In the

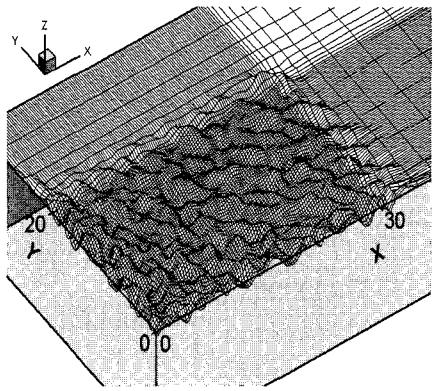

Fig. 7 3D snap-shot of wave configuration for multi-directional waves at t=50s, which are generated by DWT

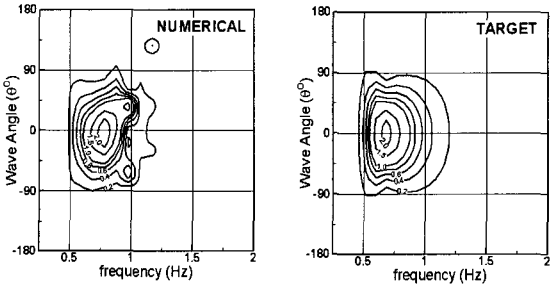

Fig. 8 Comparison of target and simulated directional spectrum in energy contour map.

figure, the simulated directional energy contour is similar to the target one, which implies the possibility of numerical reproduction for random waves inside a 3D-DWT. However, the peak frequency of the DWT is slightly shifted to high frequency region, which may be resulted in insufficient numerical condition and a lack of the number of data used for spectral analysis.

3.3 NUMERICAL GENERATION OF BULL'S-EYE WAVES

The bull's-eye waves can be generated by phase control of wavemaker panels, which is based on the fact that a group of waves is propagated towards a common focusing point. The phase difference at two different segments can be determined from $\epsilon = k(r_2 - r_1)$, where k is the wave number and r is the distance from the respective segment to the common focusing point. The bull's-eye waves were designed to converge toward a focal point along the centerline. The wave height and period are 20mm and 1.44s, respectively. Fig. 9(a) shows a snapshot of the bull's-eye wave simulation. It is seen that the current method can generate the directional wave field as designed. Fig. 9(b) show the cross section of wave profile along the focus, in which the

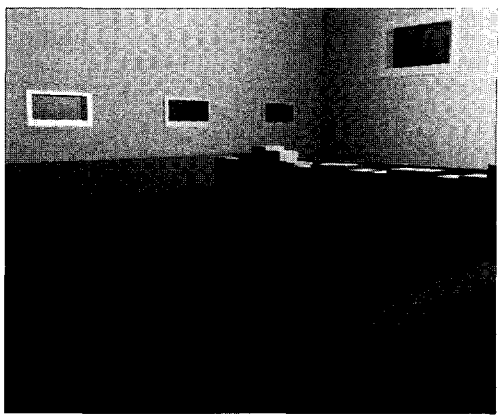

(a)

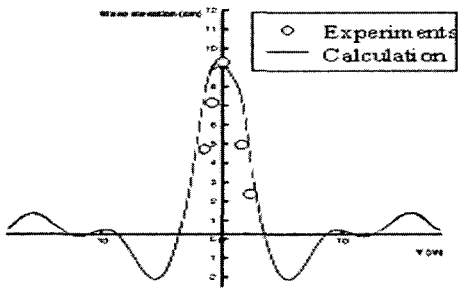

(b)

Fig. 9 Snapshot of bull's-eye wave field in a DWT (top), and cross section of wave profile along the facal point (bottom)

circle presents the experimental result conducted in the OTRC wave basin at Texas A&M University. We can see that most wave energy propagates toward the focal point, so wave amplitudes are very high there but small else where. In this simulation, the maximum wave height probed at a focal point was 9-times higher than the incident wave amplitude.

4. SOME APPLICATIONS OF FULLY NONLINEAR WAVE MOTIONS

4.1 FULLY NONLINEAR WAVE MOTIONS AROUND OFFSHORE STRUCTURES

A finite-difference method is described for 3D wave breaking phenomena. It is time-marching solution methods based on the N-S equation in the framework of an inflexible Cartesian coordinate system. The technique that makes use of the MDF is employed for such problem. Not only the overturning motion of the wave front but also the impingement of the wave front on

the surface below and vortex generation can be simulated. The availability of the method is demonstrated by the simulations of wave motions interacting with a semi-submerged body, a vertical truncated cylinder and an Arctic structure.

A part of an oil-drilling platform of the semi- submergible type is used for the simulation. By the use of the periodic condition on the side boundaries the interaction between a number of vertical pipes are considered. A 1/70 scale model is assumed and the length of the lower-hull is 0.6m and the diameter of the pipe is 0.216m. Gravity waves are periodically generated with the length and amplitude 4.2m and 0.09m respectively at the inflow boundary. The total number of grids is about 400,000 and the time-increment is 1/2400 of the wave period. The Keulegan-Carpenter (KC) number for the vertical pipe is 1.10.

The generation of 3D hydraulic jump, secondary wave crest caused by interaction and wave breaking are observed around the vertical cylinder (especially behind the cylinder). The secondary wave crest behind the vertical pipe show good agreement with the experimental observation in Fig. 10. The contours of the velocity component in the direction of wave propagation are shown on a vertical plane in Fig. 11. By the diffraction and breaking of waves as well as viscous motions a very complicated flow field is generated.

The present DWT simulations with a stationary vertical truncated cylinder (radius r=23m, draftd=1.34m) are compared with the Mercier and Niedzwecki's experiments (1994) conducted the OTRC 3D wave basin ($50 \times 33 \times 6m^3$) located at Texas A&M University. The simulation with a wave period T=1.0(sec) and the wave steepness H/L=1/21 is performed. The Reynolds number is about 105 and the KC number 1.

Fig. 12 shows two snapshots of the free-surface profiles around the vertical cylinder. The right figure is the case when the wave crest hits the weather side of the cylinder. Subsequently, the crest line splits, travels along each side, and then collides and shoots up behind the cylinder, as can be seen in the left figure. This kind of free-surface flow pattern around a vertical cylinder can also be observed in experiments, as reported in Miyata and Park (1995).

In an arctic environment, conical gravity platforms have been used to effectively break ice sheets for the reduction of ice loads. In the design of such structures, it is of significant importance to accurately predict the maximum wave run-up around the structure to determine suitable air-gap. Sufficient

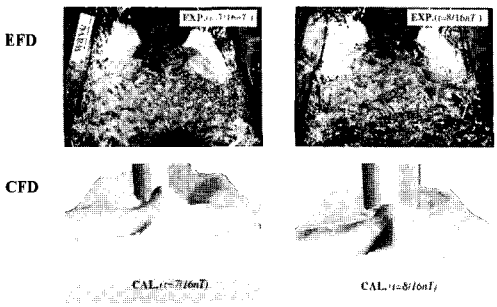

Fig. 10 Extremely Nonlinear Wave configurations near the rear part.

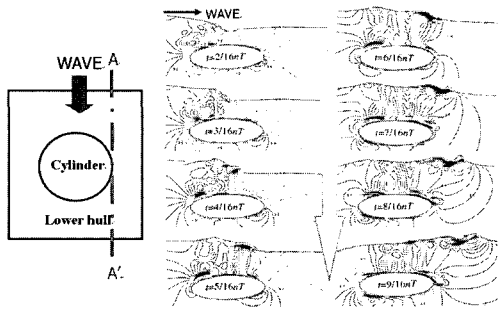

Fig. 11 Time-development of contours of longitudinal velocity component on the vertical center-plane A-A', the interval is 0.1.

T=1.0(sec), H_0/λ=1/21

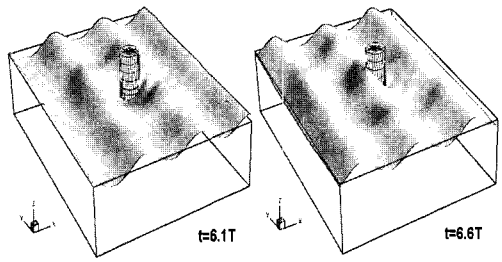

Fig. 12 Fully-Nonlinear Wave Configuration around a vertical truncated cylinder.

air-gap is required to avoid wave slamming beneath the deck.

The DWT technique is applied to nonlinear wave interactions with conical gravity platforms of circular and octagonal cross-sections as shown in Fig. 13. The numerical predictions of maximum wave run-up at the weather side are compared with the prediction of the Shore Protection Manual (SPM) method (Gadd et al., 1985) and those of linear and second-order diffraction analyses based on potential theory (Kim and Yue, 1989), in Fig. 14. Through this comparison, it seems that the

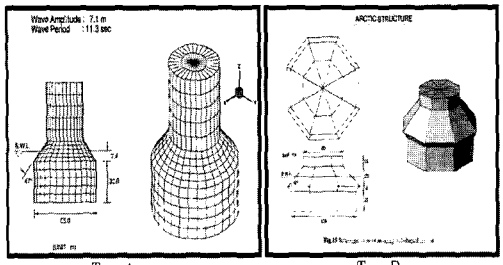

Fig. 13 Two types of Arctic structure designed by Exxon

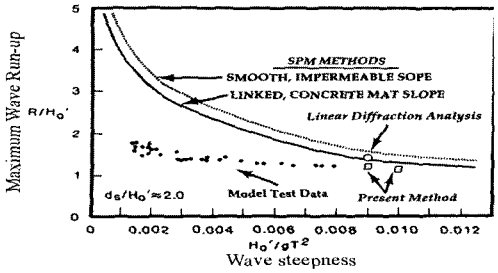

Fig. 14 Comparison of Wave Run-up on Weather Side.

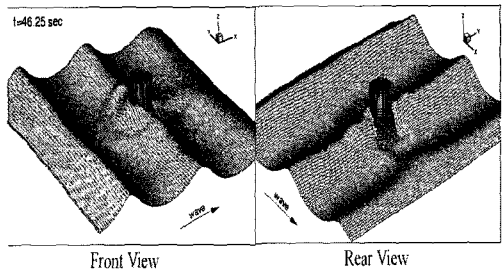

Fig. 15 A 3D snapshot of wave configuration for type B.

present DWT prediction agrees well with the model test results under the given wave condition, while the potential-based linear diffraction analysis tends to overestimate and be similar to the conventional SPM curves for impermeable slopes. 3D snap-shot of wave motions is illustrated in Fig. 15. It is observed that short ring-like waves are formed around the structure, which are believed to be the second-order free waves whose wavelength is about 1/4 of the incident wavelength. Those complicated wave motions ought to affect the nonlinear hydrodynamic forces and moments on the structure.

4.2 WAVES GENERATED BY HIGH SPEED VESSELS

A numerical simulation is performed for the 3D flow around a Wing-In-Ground (WIG) effect ship with a complex geometry,

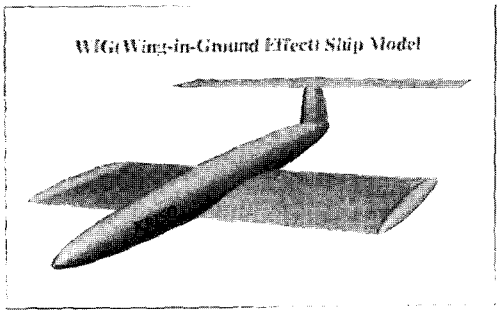

Fig. 16 A Wing-In-Ground(WIG) ship.

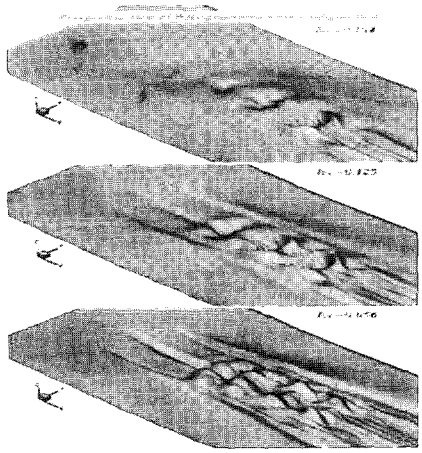

Fig. 17 Waves generated by a WIG ship.

as shown in Fig. 16. The air and water flows are simultaneously simulated in the time-marching solution procedure. The numerical calculations around a WIG ship advancing in calm water are conducted and the flow characteristics for the nonlinear wave motions generated by a WIG ship can be discussed.

The perspective views of the WIG-generated waves are shown in Fig. 17, in which wave heights are enlarged 5000 times vertically. As the altitude ratio decreases, waves are complicatedly developed and propagated to the downstream while the wave propagation in the lateral direction is restrained due to the existence of the side-endplate.

4.3 SHIP MOTIONS IN WAVES

A finite-volume method has been developed for the ship motion simulation in waves. The motion of the ship is treated in a fixed coordinate system, which means that the grid system also moves according to the ship's motion, as shown in Fig. 18. The origin of the coordinate system is at the center of the ship, and the trajectory and attitude of the ship are determined in the

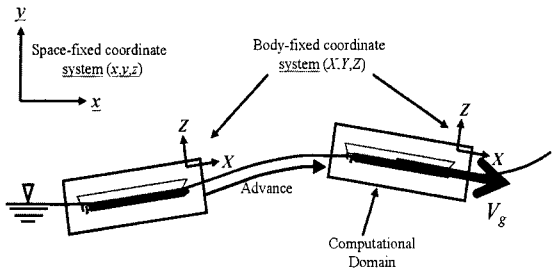

Fig. 18 Govering Equations for motion simulation.

Navier-Stokes Equation

$$\frac{\partial \mathbf{u}}{\partial t} + \nabla(\mathbf{u}-\mathbf{v})\mathbf{u} = -\nabla\phi + \nu\nabla\left[\nabla\mathbf{u} + (\nabla\mathbf{u})^{T}\right] - \overline{\mathbf{u}'\mathbf{u}'} + \underbrace{\mathbf{K}}_{\text{External Forces}}$$

$$\mathbf{K} = \underbrace{-2\omega\times\mathbf{u}}_{\text{Coliolis Force}} \underbrace{-\omega\times(\omega\times\mathbf{r})}_{\text{Circumferential Force}} \underbrace{-\frac{d\omega}{dt}\times\mathbf{r}}_{\text{Angular Acceleration}} \underbrace{-\frac{dV_t}{dt}}_{\text{Translational Acceleration}}$$

Continuity Equation

$$\nabla\mathbf{u} = 0$$

Fig. 19 Govering Equations for motion simulation.

space-fixed coordinates. The solution procedure for the Navier-Stokes equation is combined with that for the motion equations in six degree-of-freedom. The O-H type grid system surrounds the hull is employed and the motion of the structure is represented by external forces in the Navier-Stokes equation as shown in Fig. 19.

Fig. 20 shows the 3-D snapshots of the large amplitude of roll motion of a Series 60 model (Cb=0.6) advancing at Froude number 0.2 in oblique following waves of $\lambda/L=2$, $H/L=0.012$, oblique angle=20^0. In this simulation, 3-degree-of-freedom motion (Heave, Pitch and Roll motions are free). The very unstable ship motions with over the 20degrees of rolling are observed caused by following and quartering waves. However, this simulation is not continued any longer due to the grid system problem using a moving coordinate.

To handle in convenient the ship motion with large amplitude, a composite grid system is employed, which an inner O-H grid system including the ship model is overlapped onto the DWT (outer grid system) as shown in Fig. 21(left). By use of this grid system, the marine environments and ship motions are treated in two separated grid systems, which the marine environments for waves, tide, wind, etc. are generated in the outer grid system and the large motions of ship is treated by moving and rotating the whole of the inner grid system.

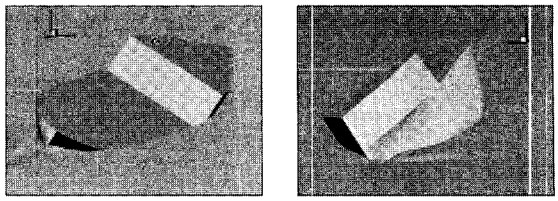

Fig. 20 3D snapshots of Series 60 model advancing in oblique following sea(left : front view, right : rear view)

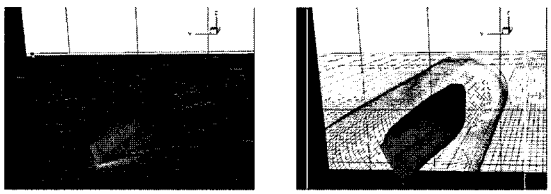

Fig. 21 Motion simulation of a Series 60 ship advancing and rolling with large amplitude (left : composite grid system, right : wave contour)

However, the numerical technique for interface where two grid systems are overlapped is quite important and must be carefully treated conserving the mass and flux on it. In the present method, a linear interpolation technique was tested and used. Ultimate Goals of the present method are to simulate the extremely nonlinear ship motion, i.e. Slamming and Capsizing motions in large-amplitude waves. In Fig. 21, Motion simulation using a composite grid system is examined for a Series 60 ship advancing at Fn=0.316 in still-water with 20 degrees of enforced roll motion.

4.4 MARINE FLOW SIMULATION WITH FREE-SURFACE

Here, such tide-induced jets over constant bathymetry are investigated numerically. In order to generate a jet in a tide-like oscillating flow, an enclosed rectangular breakwater, which has vertical opening and a large enclosed volume inside, known as a Tidal-Jet Generator (TJG), is introduced into a flow. The TJG is installed at the head of a rectangular bay. The forcing tide is given by imposing a sinusoidally varying water level at the entrance of bay. During both phases of tide, strong and uni-directional jets can be obtained locally from the inlet of the TJG, due to the water level difference between the inner and outer sides of breakwater.

Fig. 22 shows the depth-averaged momentum distribution of residual flow for three different openings ϵ;5, 15and 25(cm). The depth-averaged momentum was obtained by taking the absolute value of there sidual flow velocity remained during a

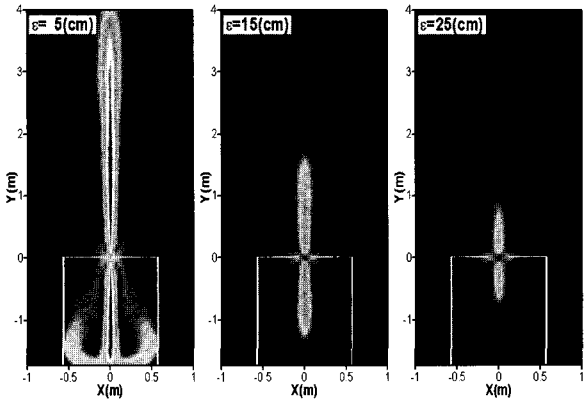

Fig. 22 Momentum distribution of residual flow around Tidal-jet-Generator.

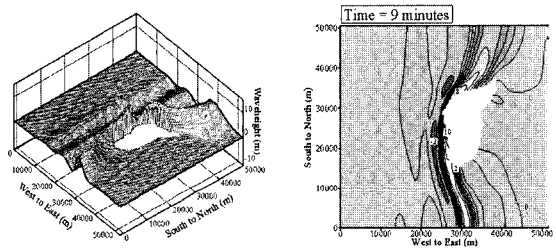

Fig. 23 Time sequences of Tsunami proparation attacking Okushiri islands (left : 2D contour, right : 3D snapshot)

tidal motion. As the opening gets small the momentum is distributed widely and strongly in the vicinity of the TJG, in which the high values are represented in the area where the tidal jet motion is occurred violently. Also, the maximum intensity of the jets can numerically be predicted and the relating processes of the jets are reproduced, and the sediment transport mechanism can be understood widely solving a scalar transport equation of such concentration.

The developed DWT simulation can be applied to the prediction of natural disaster such like inundation caused by nearshore tsunami. In this simulation the DWT solver is combined with Geographic Information System (GIS) software, named "ArcView", to generate the computational grids for real sea topology. In Fig. 23, a snap-shot for tsunami propagation attacking Okushiri Island located at the southwestern coast of Hokkaido, Japan. In the simulation, as an initial profile of tsunami is assumed to be a planer tsunami profile such like a planer solitary wave, and that is propagated from the Westside of the Island. The wave height of the tsunami is set to 4.9m and the wave period 4 minutes. The horizontal cell size is 300m and the time increment is 0.2 seconds. From the figure, it is observed the wave motions are dynamically simulated when the tsunami is attacking the Island.

5. CONCLUDING REMARKS

A DWT simulation technique based on the CFD has been developed in order to elucidate nonlinear physical phenomena and in order to design such marine systems with high performance.

In this paper, some applications for various engineering problems with free-surface were introduced and discussed. It included numerical simulation of marine environments by simulation equipments, fully nonlinear wave motions around offshore structures, nonlinear ship waves, ship motions in waves and marine flow simulation with free-surface.

In near future, the developed technology will be applied usefully to multipurpose research in marine environmental engineering fields.

REFERENCES

[1] Brackbill, J.U., Kothe, D.B. and Zemach, C., 1992, "A Continuum Method for Modeling Surface Tension," *J. of Comp. Physics*, 100, pp.335-354.

[2] Chan, R.K.C. and Street, R.L., 1970, "A Computer Study of Finite Amplitude Water Waves," *J. of Comp. Physics*, 6, pp.68-94.

[3] Dean, R.G. and Dalrymple, R.A., 1991, "Water Wave Mechanics for Engineers and Scientists," *World Scientific Publ.*

[4] Gadd, P.E., Machemehl, J.L. and Manikian, V., 1985, "Comparison of Wave Overtopping Prediction to Measurements from Large-Scale Model Tests," Proc. the Conference Arctic'85, *Civil Engineering in the Arctic Offshore*, ASCE, San Francisco, pp.698-705.

[5] Goda, Y., 1987, "Standard Spectra and Statistics of Sea Waves Derived by Numerical Simulation," *34th Japanese Conf. on Coastal Engineering*, pp.131-135.

[6] Goda, Y. and Suzuki, Y., 1975, "Computation of Refraction and Diffraction of Sea Waves with Mitsuyasu's Directional Spectrum," *Technical Note of Port and Harbor Research Institute*, No.230, pp.1-45.

[7] Hashimoto, N., Nagai, T. and Asai, T., 1994, "Extension of Maximum Entropy Principle Method (MEP) for Estimating Directional Wave Spectrum," *24th Int. Conf. Coastal*

Engineering, 1, pp.232-246.

[8] Hirt, C.W. and Nichols, B.D., 1981, "Volume of Fluid VOF Method for the Dynamics of Free Boundaries," *J. of Comp. Physics*, 39, pp.201-225.

[9] Kanai, A and Miyata, H., 2001, "Direct numerical simulation of wall turbulent flows with microbubbles," *Int. J. for Numerical Methods in Fluids*, 35, pp.593-615.

[10] Kim, M.H., Niedzwecki, J.M., Roesset, J.M., Park, J.C., Hong, S.Y. & Tavassoli, A., 2001, "Fully Nonlinear Multdirectional Waves by a 3-D Viscous Numerical Wave Tank," *J. of Offshore Mechanics and Arctic Engineering*, 123, pp.124-133.

[11] Kim, M.H., Park, J.C. and Tavassoli, A., 2000, "Fully Nonlinear Multi-directional Wave Simulations by 3D Numerical Wave Tanks," *Proc. 14th Int. Conf. on Hydrodynamics*, Yokohama.

[12] Kim, M.H. and Yue, D.K.P., 1990, "The complete second-order diffraction solution for an axisymmetric body. Part 2. Bichromatic incident waves and body motions," *Journal of Fluid Mechanics*, 211, pp.557-593.

[13] Kim, M.H. and Yue, D.K.P, 1989, "The complete second-order diffraction solution for an axisymmetric body. Part 1. Monochromatic incident waves," *Journal of Fluid Mechanics*, 200, pp.235-264.

[14] Levich, V.G. and Krylov, V.S., 1969, "Surface-Tension-Driven Phenomena," *Annual Rev. Fluid Mech.*, 1, pp.293.

[15] Mercier, R.S. and Niezwecki, J.M., 1994, "Experimental Measuremnt of Second Order Diffraction by a Truncated Vertical Cylinder in Monochromatic Waves," *Proc. 7th Intl. Conf. Behavior of Offshore Structures*, 2, pp.265-287.

[16] Miyata, H., Katsumata, M., Lee, Y.G. and Kajitani, H., 1988, "A Finite-Difference Simulation Method for Strongly Interacting Two-Layer Flow," *J. of Marine Science and Technology*, 163, pp.1-16.

[17] Miyata, H., Kanai, A. Kawamura, T. and Park, J.C., 1996, "Numerical simulation of three-dimensional breaking waves," *J. of Marine Science and Technology*, 1, pp.183-197.

[18] Miyata, H. and Park, J.C., 1995, "Ch.5 Wave Breaking Simulation," Advances in Fluid Mechanics, Potential Flow of Fluids, ed. M. Rahman, *Computational Mechanics Publications*, UK., pp.149-176.

[19] Miyata, H. and Yamada, Y., 1992, "A Finite Difference Method for 3D Flows about Bodies of Complex Geometry in Rectangular Co-ordinate Systems," *Int. J. for Numerical Methods in Fluids*, 14, pp.1261-1287.

[20] Orihara, H. and Miyata, H., 2000, "Numerical Simulation Method for Flows About a Semi-Planing Boat with a Transom Stern," *J. of Ship Research*, 44-3, pp.170-185.

[21] Park, J.C., Kim, M.H. and Miyata, H., 1999, "Fully Non-linear Free-Surface Simulations by a 3D Viscous Numerical Wave Tank," *Int. J. for Numerical Methods in Fluids*, 29, pp.685-703.

[22] Park, J.C., Kim, M.H. and Miyata, H., 2003, "Fully nonlinear numerical wave tank NWT simulations and wave run-up prediction around 3-D structures," *Ocean Engineering*, 30, pp.1969-1996.

[23] Park, J.C. and Miyata, H., 2001, "Numerical Simulation of Fully-Nonlinear Wave Motions around Arctic and Offshore Structures," *J. Soc. Naval Architecture of Japan*, 189, pp.13-19.

[24] Park, J.C. and Miyata, H., 1994, "Numerical Simulation of the Nonlinear Free-Surface Flow Caused by Breaking Waves," *ASME FED*-vol.181, Free-Surface Turbulence, pp.155-168, LakeTahoe.

[25] Park, J.C., Zhu, M. and Miyata, H., 1993, "On the Accuracy of Numerical Wave Making Techniques," *J. Soc. Naval Architecture of Japan*, 173, pp.35-44.

[26] Sato, Y., Miyata, H. and Sato, T., 1999, "CFD Simulation of 3D Motion of a Ship in Waves," *J. of Marine Science and Technology*, 4, pp.108-116.

[27] Sussman, M., Smereka, P. and Osher, S., 1994, "A Level Set Approach for Computing Solutions to Incompressible Two-Phase Flow," *J. of Comp. Physics*, 114, pp.146-159.

[28] Yabe, T., Xiao, F. and Wang, P., 1993, "Description of Complex and Sharp Interface during Shock Wave Interaction with Liquid Drop," *J. of Phys. Soc. Japan*, 62, pp.2537-2540